Journal of Pathology
J Pathol 2007; **212**: 91–101
Published online 23 March 2007 in Wiley InterScience
(www.interscience.wiley.com) **DOI:** 10.1002/path.2154

Original Paper

Morphological features of *TMPRSS2–ERG* gene fusion prostate cancer

J-M Mosquera,[1,2] S Perner,[1,2,3] F Demichelis,[1,2,4] R Kim,[1] MD Hofer,[1,2] KD Mertz,[1,2] PL Paris,[5] J Simko,[5] C Collins,[5] TA Bismar,[6] AM Chinnaiyan[7] and MA Rubin[1,2,8,9]*

[1]*Department of Pathology, Brigham and Women's Hospital, Boston, MA, USA*
[2]*Harvard Medical School, Boston, MA, USA*
[3]*University of Ulm, Department of Pathology, Ulm, Germany*
[4]*ITC-irst, SRA Division, Bioinformatics Group, Povo, Trento, Italy*
[5]*Comprehensive Cancer Center, University of California, San Francisco, CA, USA*
[6]*Departments of Pathology and Oncology, McGill University Faculty of Medicine, Montreal, QC, Canada*
[7]*Departments of Pathology and Urology, University of Michigan, Ann Arbor, MI, USA*
[8]*Broad Institute of MIT and Harvard Medical School, Cambridge, MA, USA*
[9]*Dana Farber Harvard Comprehensive Cancer Center, Boston, MA, USA*

**Correspondence to:*
Dr MA Rubin, Department of Pathology, Brigham and Women's Hospital/Harvard Medical School, 221 Longwood Avenue, EBRC 442A, Boston, MA 02115-6110, USA.
E-mail: marubin@partners.org

No conflicts of interest were declared.

Received: 12 October 2006
Revised: 18 January 2007
Accepted: 3 February 2007

Abstract

The *TMPRSS2–ETS* fusion prostate cancers comprise 50–70% of the prostate-specific antigen (PSA)-screened hospital-based prostate cancers examined to date, making it perhaps the most common genetic rearrangement in human cancer. The most common variant involves androgen-regulated *TMPRSS2* and *ERG*, both located on chromosome 21. Emerging data from our group and others suggests that *TMPRSS2–ERG* fusion prostate cancer is associated with higher tumour stage and prostate cancer-specific death. The goal of this study was to determine if this common somatic alteration is associated with a morphological phenotype. We assessed 253 prostate cancer cases for *TMPRSS2–ERG* fusion status using an *ERG* break-apart FISH assay. Blinded to gene fusion status, two reviewers assessed each tumour for presence or absence of eight morphological features. Statistical analysis was performed to look for significant associations between morphological features and *TMPRSS2–ERG* fusion status. Five morphological features were associated with *TMPRSS2–ERG* fusion prostate cancer: blue-tinged mucin, cribriform growth pattern, macronucleoli, intraductal tumour spread, and signet-ring cell features, all with p-values <0.05. Only 24% ($n = 30/125$) of tumours without any of these features displayed the *TMPRSS2–ERG* fusion. By comparison, 55% ($n = 38/69$) of cases with one feature (RR = 3.88), 86% ($n = 38/44$) of cases with two features (RR = 20.06), and 93% ($n = 14/15$) of cases with three or more features (RR = 44.33) were fusion positive ($p < 0.001$). To our knowledge, this is the first study that demonstrates a significant link between a molecular alteration in prostate cancer and distinct phenotypic features. The strength of these findings is similar to microsatellite unstable colon cancer and breast cancer involving *BRCA1* and *BRCA2* mutations. The biological effect of *TMPRSS2–ERG* overexpression may drive pathways that favour these common morphological features that pathologists observe daily. These features may also be helpful in diagnosing *TMPRSS2–ERG* fusion prostate cancer, which may have both prognostic and therapeutic implications.

Keywords: fluorescence *in situ* hybridization (FISH); translocation; gene fusion; blue-tinged mucin; cribriform growth pattern; intraductal tumour spread; signet-ring cell features; collagenous micronodules; macronucleoli

Introduction

Through careful characterization of tumours with specific chromosomal or molecular genetic aberrations, it is now clear that, conversely, the morphological phenotype of a tumour may suggest an underlying genotype. For example, microsatellite unstable colorectal cancer as seen in hereditary non-polyposis colorectal cancer is characterized by poorly differentiated tumour cells, an expanding growth pattern with pushing borders, a pronounced lymphocytic reaction with tumour-infiltrating lymphocytes, and the lack of dirty necrosis [1–5]. Breast cancer associated with *BRCA1* germline mutations frequently shows a higher mitotic rate, greater areas of the tumour with continuous pushing margins, and more lymphocytic infiltrate than sporadic

cases. Breast cancer associated with *BRCA2* mutations tends to have more tubule formation, greater areas of the tumour with continuous pushing margins, and lower mitotic count than sporadic cases [6,7]. More recently, it has also been recognized that basal-like breast carcinomas and translocation carcinomas of the kidney show a combination of morphological features that can predict the presence of underlying genetic aberrations [12–16].

Several pathological criteria are considered useful in the diagnosis of prostate cancer, including the presence of intraluminal blue-tinged mucin, intraluminal crystalloids, enlarged nuclei, prominent nucleoli, amphophilic cytoplasm, collagenous micronodules, glomerulations, and perineural invasion [17]. Of these, the last three have been considered highly specific and helpful in the diagnosis of limited prostate cancer in needle core biopsies [8–11]. At the molecular level, numerous genetic alterations have been characterized in prostate cancer, including *PTEN* loss, *c-myc* amplification, and germline susceptibility genes (eg 8q24 risk allele) [18,19]. Yet, none of these somatic or germline alterations have been associated with a specific constellation of morphological features (ie phenotype).

Recently, a common gene fusion in prostate cancer was identified that brings the androgen regulated gene *TMPRSS2* (21q22.3) and an *ETS* transcription factor family member together, either *ERG* (21q22.2), *ETV1* (7p21.2) or *ETV4* (17q21) [20,21]. Among these, the *TMPRSS2–ERG* fusion is the most prevalent, occurring in up to 50% of clinically localized prostate cancers in hospital-based cohorts [22,23]. Given the high incidence of prostate cancer [24], the *TMPRSS2–ERG* fusion is likely to be one of the most common somatic genomic alterations yet identified in any human malignancy. These observations have now been confirmed by other investigators on other surgical case series [25–27]. A significant addition to the evolving story of *TMPRSS2–ERG* fusion prostate cancer has been the recent identification of a significant association between *TMPRSS2–ERG* fusion prostate cancer, and prostate cancer-specific death [28].

The current study demonstrates for the first time a significant association between *TMPRSS2–ERG* fusion prostate cancer and a subset of commonly observed histological features.

Materials and methods

Study population

The analysis involved 227 cases of clinically localized prostate cancer from five hospital-based radical prostatectomy cohorts. The prostate cancer samples were embedded in five tissue microarrays (TMAs). One to 12, 0.6 mm in diameter TMA biopsy cores (median 3) were randomly taken from the dominant tumour nodule. To assess for homogeneity of *TMPRSS2–ERG* fusion, 26 prostate cancer-positive needle core biopsies, 9 prostatectomies, and 1 transurethral resection of prostate sample were also evaluated. All tissue samples were collected with institutional review board approval. The clinical and pathological demographics for the 227 patients with clinically localized prostate cancer represented in the TMAs have been previously described [23]. In brief, the mean age at presentation was 63 years with a mean pre-operative prostate-specific antigen (PSA) of 18.5 ng/ml. There were 25% Gleason grade $\leq$6, 36% Gleason grade 7, and 39% Gleason grade $\geq$8. The break down of pathological stage (pT) was 48% pT2, and 52% pT3.

Pathological analysis

All cases were reviewed by two pathologists (J-MM and SP). Inclusion in this study required at least one assessable TMA histospot in step sections for the haematoxylin and eosin (H&E) and fluorescence *in situ* hybridization (FISH) slides. Morphological features were evaluated blinded to the *TMPRSS2–ERG* fusion status. Assessment of common morphological features of prostate cancer included intraluminal features (blue-tinged mucin), nuclear features (macronucleoli), architectural features (intraductal tumour spread, cribriform growth pattern), malignant-specific features (extraprostatic extension, perineural invasion, glomerulations, and collagenous micronodules), histological variants (signet-ring cell features, foamy gland morphology), and comedonecrosis. The Gleason score for each TMA was assessed as previously described [29]. Histological subtypes in addition to acinar prostate cancer included ductal adenocarcinoma and small cell carcinoma [17,30]. Table 1 summarizes these features with their diagnostic and clinical significance.

In a subset of cases with equivocal diagnosis, and to distinguish intraductal tumour spread from cribriform prostate cancer, immunohistochemistry for prostatic basal cells was performed. For this purpose, serial paraffin sections were cut and set on coated slides. Subsequently, they were deparaffinized in xylene and rehydrated in graded ethanols. Pressure-cooking was applied as antigen retrieval method. Primary antibodies against p63 (1 : 50 dilution of clone 4A4, NeoMarkers, Fremont, CA, USA) and high molecular weight cytokeratin (1 : 200 dilution of clone 34βE12, DAKO, Carpinteria, CA, USA) for the detection of basal cells were applied with over night incubation at 4 °C in a humid chamber. A similar protocol was used to detect MUC1 protein in 111 cases contained in the TMAs (1 : 600 dilution of clone Ma552, Novocastra Laboratories Ltd, Newcastle upon Tyne, UK). Immunostaining was performed with the avidin–biotin peroxidase technique [31].

Table 1. Significance of morphological features, histological variants, and subtypes of prostate cancer cases assessed in the study

Feature/variant/ subtype	Diagnostic and clinical significance	Reference
Blue-tinged mucin	Intraluminal content more commonly seen in prostate cancer than mimickers such as adenosis and atrophy	Epstein and Fynheer, 1992 [46] Goldstein *et al*, 1995 [47] Ro *et al*, 1988 [48]
Macronucleoli	Helpful feature establishing diagnosis of prostate cancer. Nucleoli may also be seen in benign reactive glands	Helpap, 1998 [49]
Intraductal tumour spread	Represents an advanced stage of prostate cancer progression and is often associated with high-grade tumour. Intraductal tumour spread in needle biopsies is frequently associated with poor prognostic parameters at time of radical prostatectomy	McNeal and Yemoto, 1996 [41] Cohen *et al*, 2000 [42] Guo and Epstein, 2006 [43]
Cribriform growth pattern	Often has a prominent intraductal component, and biologically behaves more like Gleason pattern 4. Invariably found in association with other patterns of adenocarcinoma	McNeal *et al*, 1986 [40] Amin *et al*, 1994 [50] Rubin *et al*, 1998 [30] Epstein *et al* and the ISUP Grading Committee, 2005 [51]
Extraprostatic extension	Places a tumour in pT3 category on TNM classification. There is strong association between extraprostatic extension and volume, grade, pathological stage, and rate of recurrence after radical prostatectomy	Wheeler *et al*, 1998 [52] Epstein *et al*, 1993 [53]
Perineural invasion	Diagnostic criterion of prostate cancer. Present in 20% of needle biopsies	Bastacky *et al*, 1993 [54] Ali and Epstein, 2005 [55]
Glomerulations	Diagnostic criterion of prostate cancer. Grading of these structures is controversial	Baisden *et al*, 1999 [8] Epstein *et al* and the ISUP Grading Committee, 2005 [51]
Collagenous micronodules	Diagnostic criterion of prostate cancer. Tumour should be graded based on the underlying glandular architecture	Baisden *et al*, 1999 [8] Bostwick *et al*, 1995 [44] Epstein *et al* and the ISUP Grading Committee, 2005 [51]
Comedonecrosis	Gleason pattern 5 criterion. Can be present with solid nests or with cribriform masses of tumour	Epstein *et al* and the ISUP Grading Committee, 2005 [51]
Prostate cancer with signet-ring cell features	Signet-ring cells are present in 2.5% of cases of acinar prostate cancer. Associated with other forms of poorly differentiated prostate cancer. Final diagnosis of signet-ring cell prostate cancer should be assigned only upon examination of prostatectomy. It requires 25–50% of the tumour to be composed of signet-ring cells	Geurin *et al*, 1993 [56] Bostwick and Eble, 1997 [57]
Foamy gland morphology	Prostate cancer that resembles benign prostate glands and may be associated with higher tumour grade and aggressive behaviour	Nelson and Epstein, 1996 [58] Tran *et al*, 2001 [59]
Prostate cancer with ductal features	Peripherally located tumours are often admixed with other patterns of acinar prostate cancer. In pure form ductal prostate cancer accounts for only 0.2–0.8 of prostate cancer and has an aggressive behaviour. Should be graded as Gleason score $4 + 4 = 8$	Bostwick *et al*, 1985 [60] Epstein and Woodruff, 1986 [61] Epstein *et al* and the ISUP Grading Committee, 2005 [51]
Small cell carcinoma of prostate	In about 50% of cases small cell carcinoma is admixed with adenocarcinoma of the prostate. Small cell carcinoma should be specified in the diagnosis for therapeutic and prognostic implications. In pure form it should not be assigned a Gleason grade	Ro *et al*, 1987 [62] Tetu *et al*, 1987 [63] Epstein *et al* and the ISUP Grading Committee, 2005 [51]

Assessment of *TMPRSS2–ERG* fusion status using an interphase FISH assay testing for *ERG* break apart

We previously described the dual-colour interphase break-apart FISH assay to assess indirectly the fusion of *TMPRSS2–ERG*. Two differentially labelled probes were designed to span the telomeric and centromeric neighbouring regions of the *ERG* locus. As previously described, this break-apart probe system allows differentiation between *TMPRSS2–ERG* fusion through translocation, *TMPRSS2–ERG* fusion through an intronic deletion, and no gene rearrangement [21–23, 28]. Briefly, a nucleus without *ERG* rearrangement demonstrates two pairs of juxtaposed red and green signals, forming yellow fusion signals. A nucleus with an *ERG* break apart (reflecting a *TMPRSS2–ERG* fusion through translocation) shows split apart of one juxtaposed red–green signal pair, resulting in a single red and green signal for the translocated *ERG* allele, and a still combined (yellow) signal for the non-translocated *ERG* allele in each nucleus. Finally, a nucleus with deletion of the telomeric (green) *ERG* break-apart probe (reflecting a

TMPRSS2–ERG fusion through deletion) shows one juxtaposed red–green signal pair (yellow) for the non-rearranged allele, and a single red signal for the rearranged (through deletion) allele. The potential technical difficulties with this assay included the absence of diagnostic material to evaluate, weak probe signals, and overlapping nuclei preventing accurate assessment.

The samples were analysed under a ×60 oil immersion objective using an Olympus BX-51 fluorescence microscope equipped with appropriate filters, a charge-coupled device camera (Olympus, Center Valley, PA, USA), and the CytoVision FISH imaging and capturing software (Applied Imaging, San Jose, CA, USA). Evaluation of the tests was independently performed by two pathologists (J-MM and SP) with expertise in analysing interphase FISH experiments. For each case, we attempted to score at least 100 nuclei. Cases with significant differences between the results of both pathologists were refereed by a third pathologist (MAR).

Semi-automated quantitative image analysis of MUC1

The intensity of MUC1 protein expression was evaluated using a semi-automated quantitative image analysis system, ACIS II (ChromaVision, San Juan Capistrano, CA, USA), as previously described [32].

Statistical analysis

All analyses were performed using SPSS 13.0 for Windows.

Contingency tables were run for each morphological parameter and *TMPRSS2–ERG* fusion status. We evaluated sensitivity and specificity and used Fisher's exact test as statistical significance test for association. The same statistics were applied to evaluate associations between morphological features.

Logistic regression was used to evaluate the prediction of *TMPRSS2–ERG* fusion status based on morphological features. We applied forward selection with Wald statistics as the selection method. Based on the selected features, each independently significant in logistic regression, a new variable was created to characterize a model that evaluated the presence of multiple morphological features to predict *TMPRSS2–ERG* fusion compared with having none of the significant individual morphological features.

The association between MUC1 protein expression and *TMPRSS2–ERG* fusion status was assessed using the *t*-test.

For all analyses, two-tail *p*-values ≤ 0.05 were considered statistically significant.

Results

Of all the common morphological features described above, one or more was observed in 66% (167/253) of the cases, and 63% of these (105/167) were *TMPRSS2–ERG* fusion positive. The remaining 34% (86/253) of cases did not show any of the above mentioned morphological feature, and 83% of these (71/86) were fusion negative.

Eight histological features were evaluated for their association with *TMPRSS2–ERG* fusion status, including cribriform growth pattern, macronucleoli, blue-tinged mucin, intraductal tumour spread, foamy gland morphology, collagenous micronodules, signet-ring

Table 2. Association of *TMPRSS2–ERG* fusion status and morphological features

		***TMPRSS2–ERG* fusion status**				
Morphological features		**Negative (*n* = 133) No (%)**	**Positive (*n* = 120) No (%)**	**Sensitivity**	**Specificity**	***p*-Value**
Cribriform growth pattern	Negative	109 (82.0)	50 (41.7)	0.42	0.82	<0.001
	Positive	24 (18.0)	70 (58.3)			
Macronucleoli	Negative	122 (91.7)	81 (67.5)	0.33	0.92	<0.001
	Positive	11 (8.3)	39 (32.5)			
Blue-tinged mucin	Negative	129 (97.0)	97 (80.8)	0.19	0.97	<0.001
	Positive	4 (3.0)	23 (19.2)			
Intraductal tumour spread	Negative	128 (96.2)	38 (31.7)	0.32	0.96	<0.001
	Positive	5 (3.8)	82 (68.3)			
Foamy gland morphology	Negative	113 (85.0)	89 (74.2)	0.26	0.85	0.041
	Positive	20 (15.0)	31 (25.8)			
Collagenous micronodules	Negative	132 (99.2)	111 (92.5)	0.08	0.99	0.007
	Positive	1 (0.8)	9 (7.5)			
Signet-ring cell features	Negative	131 (98.5)	111 (92.5)	0.08	0.98	0.028
	Positive	2 (1.5)	9 (7.5)			
Glomerulations	Negative	131 (98.5)	115 (95.8)	0.04	0.98	0.261
	Positive	2 (1.5)	5 (4.2)			

cell features, and glomerulations. Table 2 summarizes the association between *TMPRSS2–ERG* fusion status and these morphological features. Other features and subtypes of prostate cancer that were not included in the selection are extraprostatic extension ($n = 3$), perineural invasion ($n = 14$), comedonecrosis ($n = 6$), small cell carcinoma ($n = 2$), and ductal adenocarcinoma ($n = 5$). The reason for exclusion was infrequent occurrence. For extraprostatic extension and perineural invasion, this is probably owing to the lack of representation in TMA cores.

After logistic regression analysis, the following five morphological features were shown to be associated with positive *TMPRSS2–ERG* fusion status: blue-tinged mucin, cribriform growth pattern, macronucleoli, intraductal tumour spread, and signet-ring cell features. Eighty-five per cent (23/27) of cases with blue-tinged mucin (Figures 1A and B), 68% (50/74) of cases with cribriform growth pattern (Figures 1C and D), 78% (39/50) of cases with macronucleoli, 88% (38/43) of cases with intraductal tumour spread (Figures 1E and F), and 82% (9/11) of cases with signet-ring cell features (Figures 2A and B) were *TMPRSS2–ERG* fusion positive. The presence of collagenous micronodules (Figures 2C and D) did not result as independently significant ($p = 0.056$). Glomerulations and foamy gland features were not significantly associated with gene fusion (Figures 2E and F).

Table 3 shows the final model. Each morphological feature within this model has a significant relative risk ($p < 0.05$). Table 4 illustrates the association between the number of morphological features in the best model and fusion status after logistic regression analysis. Categorical variables are considered from 0 to 3, the latter representing cases with three or more features. Level 0 (no features of best model) is used as the reference. Of 125 cases with no features included in the best model, only 24% ($n = 30$) were *TMPRSS2–ERG* fusion positive. By comparison, 55% (38/69) of cases with one feature, 86% (38/44) of cases with two features, and 93% (14/15) of cases with three or more features of the best model, were fusion positive ($p < 0.001$). The model has a sensitivity of 75% and a specificity of 71% in predicting positive *TMPRSS2–ERG* fusion status.

Cross-tabulation assessment between morphological features showed significant association between tumour intraductal spread and cribriform growth pattern ($p < 0.001$), tumour intraductal spread and collagenous micronodules ($p = 0.015$), and blue-tinged mucin and macronucleoli ($p = 0.008$). In addition, the combination of blue-tinged mucin and macronucleoli, and cribriform growth and intraductal tumour spread, were significantly associated with positive *TMPRSS2–ERG* fusion status ($p < 0.001$).

Two of three cases with extraprostatic extension, six of 14 cases with perineural invasion, and four of six cases with comedonecrosis were *TMPRSS2–ERG* fusion positive. Of non-acinar prostate cancer cases, the two small cell carcinomas were gene fusion negative, and two of five ductal adenocarcinomas were positive for the *TMPRSS2–ERG* fusion.

No significant statistical association was found between Gleason score and *TMPRSS2–ERG* fusion status.

A significant association between MUC1 protein expression and *TMPRSS2–ERG* fusion status was identified ($p = 0.019$). Figure 3 illustrates MUC1 positivity of *TMPRSS2–ERG* fusion positive prostate cancer, and the results of their association.

Discussion

The histological recognition of a tumour phenotype associated with specific genotype is an important bridge between pathology and molecular analysis. Depending on the clinical significance, these observations may become relevant for patient management. In the *TMPRSS2–ETS* fusion prostate cancer scenario, recent work has demonstrated that the *TMPRSS2–ERG* variant is associated with higher tumour stage and prostate cancer-specific death [22,26,28]. In one study that included men diagnosed with clinically localized prostate cancer in the pre-PSA era and followed with expectant management (ie watchful waiting), the presence of the *TMPRSS2–ERG* gene fusion in their diagnostic tissue was associated with either the development of prostate cancer metastases or prostate cancer-specific death, with up to 22 years of clinical follow up [28]. Similar to results of our previous studies [22,26,28], we did not identify an association between gene fusion and Gleason score. However, we did observe significant associations with some histological patterns that have been linked to more aggressive prostate cancer, such as signet-ring cell morphology and intraductal tumour spread [22,26,28], and the clinical parameters mentioned above. The *TMPRSS2–ERG* gene fusion appears to be independent of Gleason score but associated with other features linked to aggressive prostate cancer. These data suggest that in addition to a diagnostic utility, the presence of the *TMPRSS2–ERG* gene fusion may also be important prognostically. Hence the need to have reproducible morphological screening criteria to determine which prostate cancer deserves a confirmatory test (ie FISH). This current study demonstrates that the phenotype of *TMPRSS2–ERG* fusion prostate cancer includes common morphological features that pathologists observe every day.

It is well documented that other carcinomas with specific germline or somatic alterations show a combination of recognizable histopathological features. Our results for sensitivity, specificity, and relative risk are comparable with those of microsatellite unstable colon cancer and the breast cancers seen in *BRCA1* and *BRCA2* mutation carriers (Table 5). Translocation carcinomas of the kidney and basal cell-like breast carcinoma have also been associated with a combination

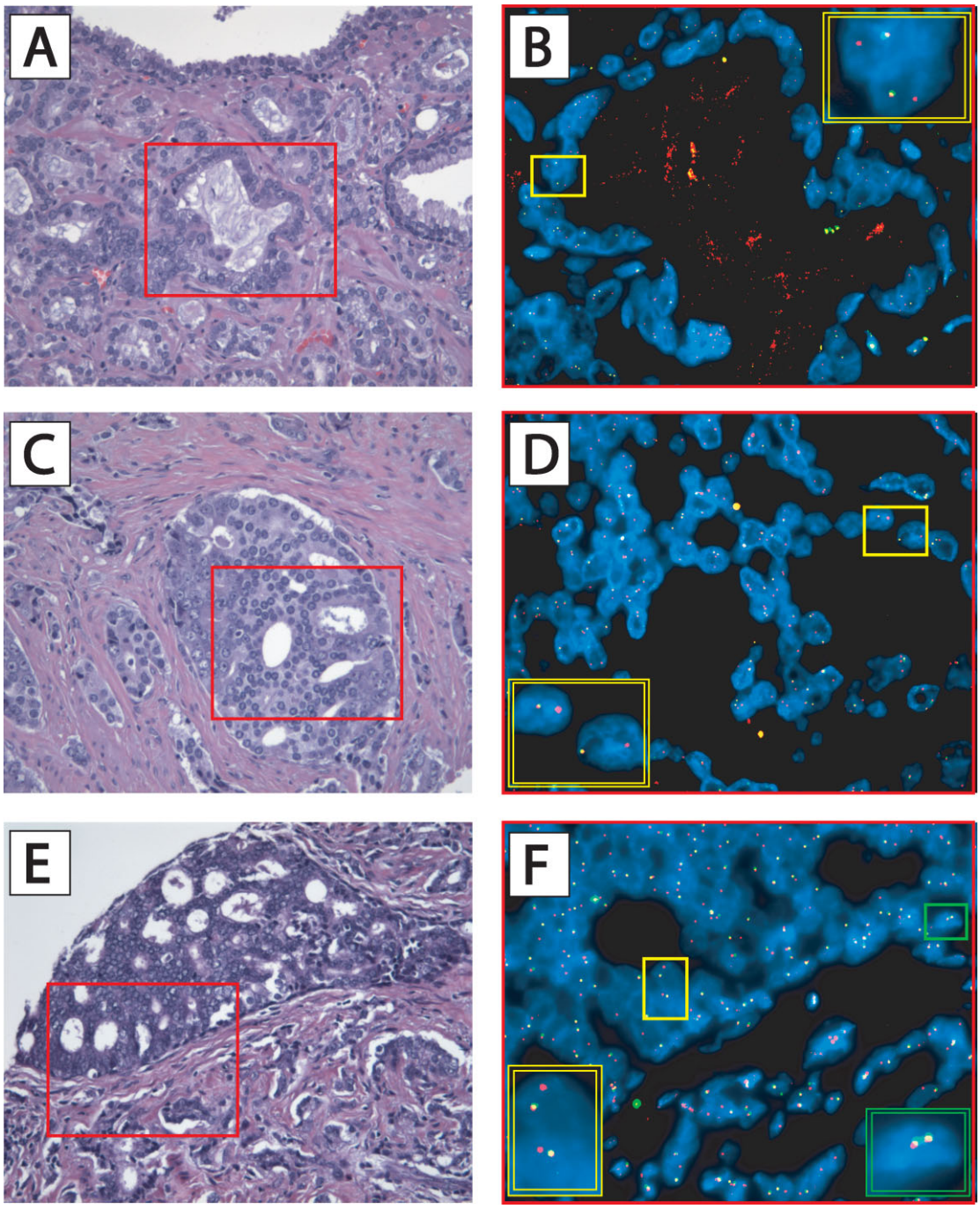

Figure 1. H&E stains and corresponding FISH images of the *TMPRSS2–ERG* fusion assay. (A) Prostate cancer Gleason pattern 3 showing blue-tinged mucin. Note benign prostatic glands at 12 and 3 o'clock. (B) FISH image of the red-boxed area in A. One yellow and one red signal are present in each nucleus, demonstrating the presence of *TMPRSS2–ERG* fusion through deletion. The double-framed yellow inset is a magnification of the yellow boxed area, showing two representative nuclei of the prostate cancer gland. (C) Prostate cancer Gleason pattern 4 with cribriform appearance. (D) FISH image of the red boxed area in C. One yellow and one red signal are present in each nucleus, demonstrating the presence of *TMPRSS2–ERG* fusion through deletion. The double-framed yellow inset is a magnification of the yellow boxed area showing two representative nuclei of the prostate cancer area. (E) Intraductal spread of prostate cancer, predominantly Gleason pattern 4. (F) FISH image of the red boxed area in E. Prostate cancer nuclei show one yellow and one red signal each, demonstrating the presence of *TMPRSS2–ERG* fusion through deletion. The double-framed yellow inset is a magnification of the yellow boxed area showing two representative nuclei of prostate cancer. In contrast, the nuclei of basal cells show two yellow signals each, demonstrating the absence of genetic aberration. The double-framed green inset is a magnification of the green boxed area showing representative nuclei of basal cells. Original magnification of H&E images, ×20 objective. Original magnification of FISH images, ×60 objective

of features that correlate with, and hence can predict, the underlying genetic aberration [12–16]. The cases of renal translocation carcinomas have been documented in smaller series, and evaluation of sensitivity and specificity of histological features has not been assessed. On the other hand, the recently published data on basal phenotype in high-grade invasive ductal carcinoma of the breast provide additional support for

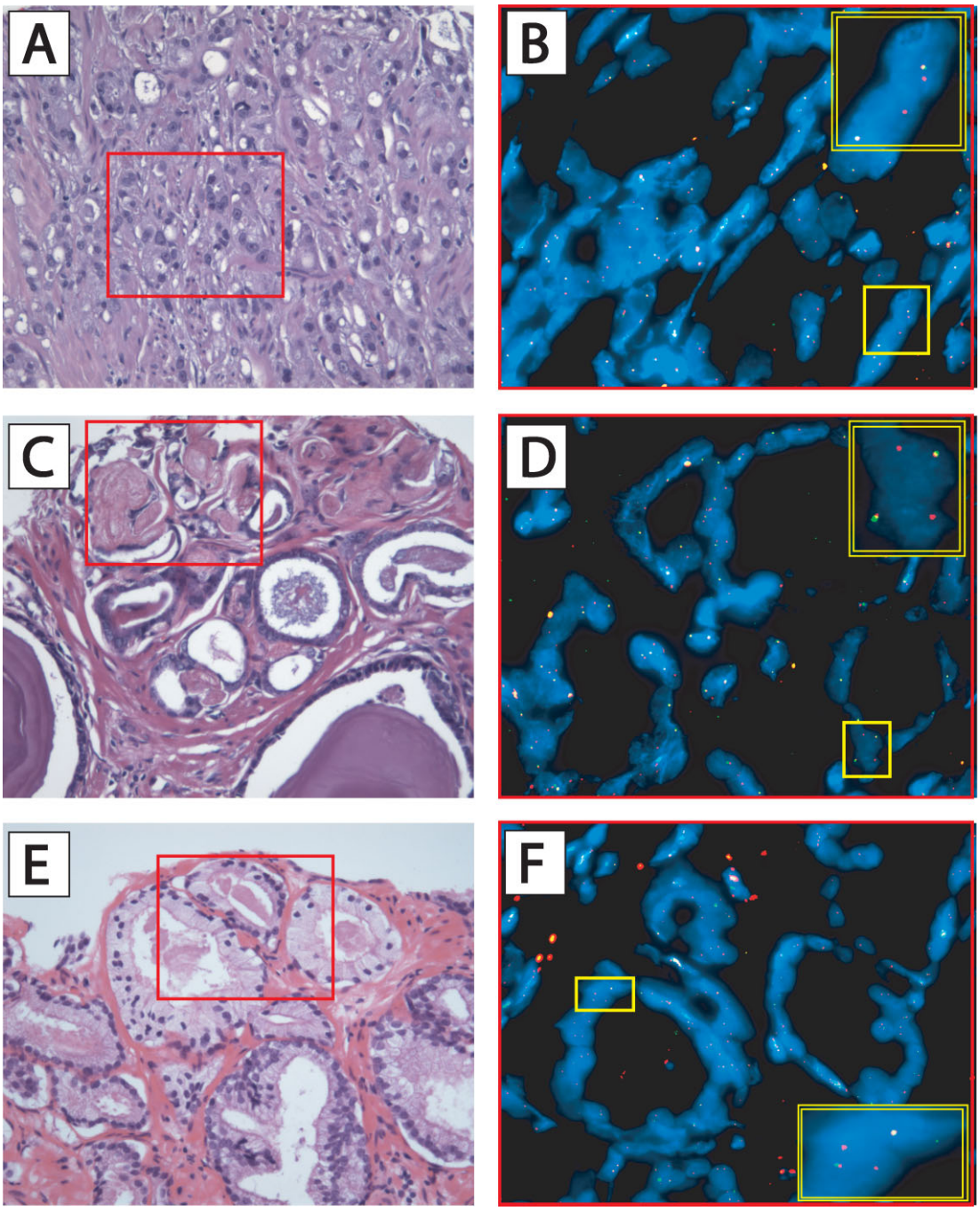

Figure 2. H&E stains and corresponding FISH images of *TMPRSS2–ERG* fusion assay. (A) Prostate cancer with Gleason patterns 4 and 5 showing focal signet-ring cell morphology. (B) FISH image of the red boxed area in A. The tumour cells show one yellow and one red signal for each nucleus, demonstrating the presence of *TMPRSS2–ERG* fusion through deletion. The double-framed yellow inset is a magnification of the yellow boxed area showing two representative nuclei of prostate cancer. (C) Prostate cancer with collagenous micronodules, Gleason patterns 3 and 4. (D) FISH image of the red boxed area in C. Tumour cells show one yellow and one red signal for each nucleus, demonstrating the presence of *TMPRSS2–ERG* fusion through deletion. The double-framed inset illustrates the magnified view of the yellow boxed area showing two representative nuclei of prostate cancer. (E) Prostate cancer with foamy gland morphology. (F) FISH image of the red boxed area in E. Prostate cancer nuclei show one yellow and one red signal each, demonstrating the presence of *TMPRSS2–ERG* fusion through deletion. The double-framed yellow inset is a magnification of the yellow boxed area showing two representative nuclei of prostate cancer. Original magnification of H&E images, ×20 objective. Original magnification of FISH images, ×60 objective

significant association between phenotype and genotype, which have implications for routine diagnostic practice and prognostication [16,33,34].

The findings in the current study might also expand our understanding of genotype/phenotype links in prostate cancer. One of the most striking findings in our study is the significant association of blue-tinged mucin with positive *TMPRSS2–ERG* fusion status. This is a quite common histological finding that, to our knowledge, has not been associated with any molecular event so far. In one study of consultation service material, intraluminal blue mucin

Table 3. Best model for morphological features associated with positive *TMPRSS2–ERG* fusion status

Morphological features	RR	95% CI lower	95% CI upper	*p* Value
Intraductal spread	8.312	2.835	24.371	0.000
Cribriform pattern	2.072	1.020	4.206	0.044
Blue-tinged mucin	5.893	1.796	19.333	0.003
Macronucleoli	4.730	2.117	10.571	0.000
Signet-ring cell	7.274	1.394	37.951	0.019

Table 4. Univariate logistic regression of best model

Number of features	Fusion negative ($n = 133$)	Fusion positive ($n = 120$)	RR	95% CI lower	95% CI lower	*p*-Value
0	95	30	REF	—	—	—
1	31	38	3.882	2.073	7.269	0.000
2	6	38	20.056	7.727	52.058	0.000
≥3	1	14	44.333	5.595	351.286	0.000

secretions were present in a third of prostate cancer cases [35]. This is exactly the same prevalence of fusion positive tumours (33%) in the clinical samples that we included in the current study (data not shown), which falls in the range of the previously described cohorts. Regarding prostate cancer progression, the presence of acidic mucins and overexpression of mucin-related genes (eg MUC1) has been linked to aggressive prostate cancer [36–38]. Remarkably, we found a significant association between MUC1 protein expression and *TMPRSS2–ERG* prostate cancer, further supporting this molecular bond. Given the parallel prevalence of *TMPRSS2–ERG* fusion and blue-tinged mucin and their significant association, as well as the aforementioned link with MUC1 expression, it is reasonable to speculate that *TMPRSS2–ERG* fusion may alter molecular pathways, favouring mucin secretion and the expression of other patterns illustrated through this study. Another example is signet-ring cell morphology, also linked to the gene fusion and previously associated with mucin production and the presence of high-grade prostate cancer [39]. Cross-tabulation analysis linked the presence of blue-tinged mucin with macronucleoli, another common histological finding that was also associated with positive fusion status.

Another remarkable finding is the significant association of *TMPRSS2–ERG* fusion prostate cancer with cribriform growth pattern and intraductal tumour spread. The latter is quite common in infiltrating cribriform acinar prostate cancer and has a unique biological significance [40,41], given the strong association with several factors contributing to increased risk of progression after prostatectomy, including high Gleason grade, large tumour volume, positive surgical margins, and extensive perineural invasion [42]. Intraductal tumour spread probably represents a late stage in tumour progression [30,43], and the *TMPRSS2–ERG* fusion is thought to be an early event in the development of invasive prostate cancer [23]. We may hypothesize that *TMPRSS2–ERG* gene fusion not only drives phenotypic expression but also may imply distinct molecular alterations leading to more aggressive behaviour [22,26,28]. The biological role of *TMPRSS2–ERG* gene rearrangement may explain prostate cancer progression. *TMPRSS2* is a tightly androgen regulated gene and the *ETS* genes of transcription factors are putative oncogenes [36–38]. In addition to the oncogenic potential of the *TMPRSS2–ERG* fusion product, loss of genes with

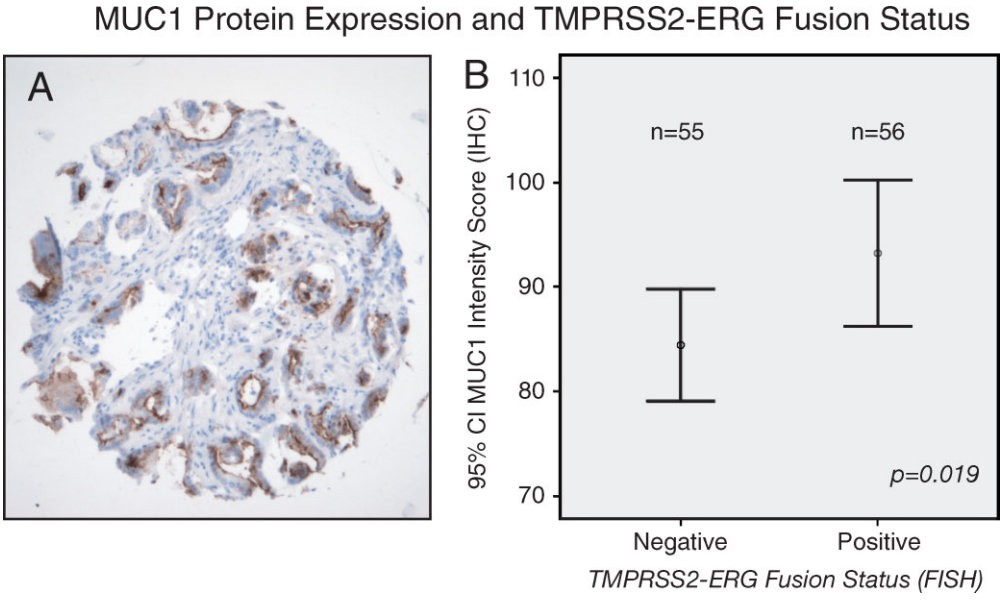

Figure 3. MUC1 immunostain and association with *TMPRSS2–ERG* fusion status. (A) Prostate cancer Gleason pattern 3 showing high MUC1 protein expression. The tumour is *TMPRSS2–ERG* fusion positive by FISH and features blue-tinged mucin and macronucleoli on H&E (not shown). (B) Significant association between MUC1 protein expression (95% confidence interval of immunostaining intensity score), and *TMPRSS2–ERG* fusion status ($p = 0.019$)

J Pathol 2007; **212**: 91–101 DOI: 10.1002/path

Table 5. Selection of different carcinomas with gene-alteration-specific morphological features

Type of carcinoma	Morphological features	Sensitivity	Specificity	Odds ratio	*p*-Value	Reference
Microsatellite unstable colon cancer	>2 TIL/HPF	0.21–0.90	0.77–0.97	9.8–16.3	<0.001	Greenson *et al*, 2003 [2], Alexander *et al*, 2001 [1]
	Absence of dirty necrosis	0.83	0.77	4.9	0.005	Greenson *et al*, 2003 [2]
	Crohn's-like inflammatory reaction	0.69	0.56	3.5	0.006	
	Any mucinous differentiation	0.22–0.67	0.82–0.93	2.7–3.7	<0.05	Greenson *et al*, 2003 [2], Alexander *et al*, 2001 [1]
BRCA1 associated breast cancer	Higher mitotic counts*	n/a	n/a	1.5–3.0	0.001	Lakhani *et al*, 1998 [7]
	Greater proportion of tumour with continuous pushing margins*	n/a	n/a	1.8–2.9	<0.001	
	More lymphocytic infiltration*	n/a	n/a	1.9–2.5	0.002	
BRCA2 associated breast cancer	Higher score for tubule formation*	n/a	n/a	5.1–13.4	<0.001	Lakhani *et al*, 1998 [7]
	Greater proportion of tumour with continuous pushing margins*	n/a	n/a	2.6–3.2	<0.001	
	Lower mitotic count*	n/a	n/a	0.1–0.9	0.003	
TMPRSS2–ERG fusion prostate cancer	Cribriform growth pattern	0.42	0.82	2.1†	0.04	Current study
	Intraductal tumour spread	0.32	0.96	8.3†	0.000	
	Blue-tinged mucin	0.19	0.97	5.9†	0.003	
	Macronucleoli	0.33	0.92	4.7†	0.000	
	Signet-ring cell features	0.08	0.98	7.3†	0.019	

* When compared with sporadic breast cancers.
† Relative risk.
n/a = not available.

tumour suppressor gene potential located in the deletion site (eg *HMGN1, Ets-2*) may be associated with even worse outcome [36–38].

One potential limitation of this study is the under-representation of certain morphological features on TMAs. Examples include collagenous micronodules, a prostate cancer-specific but infrequent diagnostic finding [44], extraprostatic extension and perineural invasion, which may have been missed, given the targeted central areas of tumour masses. Further evaluation of the significant morphological features for inter-observer agreement as well as validation on larger cohorts is needed. The main focus of the current study was to find the aforementioned morphological features of prostate cancer associated with *TMPRSS2–ERG* gene fusion, and did not explore its prevalence in high-grade prostatic intraepithelial neoplasia (PIN) or in benign lesions such as atrophy. Consistent with recently published data [45], we have found that about 20% of high-grade PIN lesions harbour the *TMPRSS2–ERG* gene fusion [23]. A follow-up study that includes a large series of prostate cancer with paired high-grade PIN lesions is currently underway.

In summary, we have demonstrated a significant association between common morphological features of prostate cancer (phenotype) and *TMPRSS2–ERG* fusion prostate cancer (genotype). The presence of any of the significant features could potentially be used to alert the pathologist to the diagnosis of a fusion positive prostate cancer. This association may also help to identify higher risk prostate cancer, impacting clinical management. Finally, these findings may help us understand specific biological pathways associated with this recently described translocation.

Acknowledgements

We thank Dr Christopher DM Fletcher for his significant discussion of the manuscript.

Research supported by the NIH Prostate SPORE at the Dana-Farber/Harvard Cancer Center NCI P50 CA090381 (MAR), R01AG21404 (MAR), Deutsche Forschungsgemeinschaft DFG# PE1179/1-2 (SP), the Prostate Cancer Foundation (FD), UCSF Prostate Cancer SPORE, NIH Grant P50CA89520 (PLP, CC, JS) and the NIH Grant UO1 CA 113913 for the BID EDRN (Harvard/Michigan Prostate Cancer Clinical Center).

We are grateful to Danielle Cullinane of the DFHCC TMA core facility, Zuned Khalifa, and Kelly Lamb for technical support critical to this study.

References

1. Alexander J, Watanabe T, Wu TT, Rashid A, Li S, Hamilton SR. Histopathological identification of colon cancer with microsatellite instability. *Am J Pathol* 2001;**158:**527–535.
2. Greenson JK, Bonner JD, Ben-Yzhak O, Cohen HI, Miselevich I, Resnick MB, *et al*. Phenotype of microsatellite unstable colorectal carcinomas: well-differentiated and focally mucinous tumors and the absence of dirty necrosis correlate with microsatellite instability. *Am J Surg Pathol* 2003;**27:**563–570.
3. Halvarsson B, Muller W, Planck M, Benoni AC, Mangell P, Ottosson J, *et al*. Phenotypic heterogeneity in hereditary non-polyposis colorectal cancer: identical germline mutations associated with variable tumor morphology and immunohistochemical expression. *J Clin Pathol* 2006;Aug 10 [Epub ahead of print].
4. Jass JR. Pathology of hereditary nonpolyposis colorectal cancer. *Ann N Y Acad Sci* 2000;**910:**62–73; discussion 73–74.
5. Lynch HT, Smyrk T, Lynch JF. Overview of natural history, pathology, molecular genetics and management of HNPCC (Lynch syndrome). *Int J Cancer* 1996;**69:**38–43.
6. Lakhani SR. The pathology of familial breast cancer: morphological aspects. *Breast Cancer Res* 1999;**1:**31–35.

7. Lakhani SR, Jacquemier J, Sloane JP, Gusterson BA, Anderson TJ, van de Vijver MJ, *et al*. Multifactorial analysis of differences between sporadic breast cancers and cancers involving BRCA1 and BRCA2 mutations. *J Natl Cancer Inst* 1998;**90:**1138–1145.
8. Baisden BL, Kahane H, Epstein JI. Perineural invasion, mucinous fibroplasia, and glomerulations: diagnostic features of limited cancer on prostate needle biopsy. *Am J Surg Pathol* 1999;**23:**918–924.
9. Epstein JI. Diagnostic criteria of limited adenocarcinoma of the prostate on needle biopsy. *Hum Pathol* 1995;**26:**223–229.
10. Epstein JI. Diagnosis and reporting of limited adenocarcinoma of the prostate on needle biopsy. *Mod Pathol* 2004;**17:**307–315.
11. Thorson P, Vollmer RT, Arcangeli C, Keetch DW, Humphrey PA. Minimal carcinoma in prostate needle biopsy specimens: diagnostic features and radical prostatectomy follow-up. *Mod Pathol* 1998;**11:**543–551.
12. Argani P, Antonescu CR, Illei PB, Lui MY, Timmons CF, Newbury R, *et al*. Primary renal neoplasms with the ASPL–TFE3 gene fusion of alveolar soft part sarcoma: a distinctive tumor entity previously included among renal cell carcinomas of children and adolescents. *Am J Pathol* 2001;**159:**179–192.
13. Argani P, Lae M, Ballard ET, Amin M, Manivel C, Hutchinson B, *et al*. Translocation carcinomas of the kidney after chemotherapy in childhood. *J Clin Oncol* 2006;**24:**1529–1534.
14. Argani P, Lae M, Hutchinson B, Reuter VE, Collins MH, Perentesis J, *et al*. Renal carcinomas with the t(6;11)(p21;q12): clinicopathologic features and demonstration of the specific alpha-TFEB gene fusion by immunohistochemistry, RT-PCR, and DNA PCR. *Am J Surg Pathol* 2005;**29:**230–240.
15. Bruder E, Passera O, Harms D, Leuschner I, Ladanyi M, Argani P, *et al*. Morphologic and molecular characterization of renal cell carcinoma in children and young adults. *Am J Surg Pathol* 2004;**28:**1117–1132.
16. Fulford LG, Easton DF, Reis-Filho JS, Sofronis A, Gillett CE, Lakhani SR, *et al*. Specific morphological features predictive for the basal phenotype in grade 3 invasive ductal carcinoma of breast. *Histopathology* 2006;**49:**22–34.
17. Eble JN, Sauter G, Epstein JI, Sesterhann IAE. *World Health Organization Classification of Tumours. Pathology and Genetics of Tumours of the Male Urinary System and Male Gential Organs*. IARC Press: Lyon, 2004.
18. Amundadottir LT, Sulem P, Gudmundsson J, Helgason A, Baker A, Agnarsson BA, *et al*. A common variant associated with prostate cancer in European and African populations. *Nat Genet* 2006;**38:**652–658.
19. Freedman ML, Haiman CA, Patterson N, McDonald GJ, Tandon A, Waliszewska A, *et al*. Admixture mapping identifies 8q24 as a prostate cancer risk locus in African-American men. *Proc Natl Acad Sci USA* 2006;**103:**14068–14073.
20. Tomlins SA, Mehra R, Rhodes DR, Smith LR, Roulston D, Helgeson BE, *et al*. TMPRSS2:ETV4 gene fusions define a third molecular subtype of prostate cancer. *Cancer Res* 2006;**66:**3396–3400.
21. Tomlins SA, Rhodes DR, Perner S, Dhanasekaran SM, Mehra R, Sun XW, *et al*. Recurrent fusion of TMPRSS2 and ETS transcription factor genes in prostate cancer. *Science* 2005;**310:**644–648.
22. Perner S, Demichelis F, Beroukhim R, Schmidt FH, Mosquera JM, Setlur S, *et al*. TMPRSS2:ERG fusion-associated deletions provide insight into the heterogeneity of prostate cancer. *Cancer Res* 2006;**66:**8337–8341.
23. Perner S, Mosquera JM, Demichelis F, Hofer MD, Paris PL, Simko J, *et al*. *TMPRSS2-ERG* fusion prostate cancer: an early molecular event associated with invasion. *Am J Surg Pathol* (in press).
24. Jemal A, Siegel R, Ward E, Murray T, Xu J, Smigal C, *et al*. Cancer statistics, 2006. *CA Cancer J Clin* 2006;**56:**106–130.
25. Soller MJ, Isaksson M, Elfving P, Soller W, Lundgren R, Panagopoulos I. Confirmation of the high frequency of the TMPRSS2/ERG fusion gene in prostate cancer. *Genes Chromosomes Cancer* 2006;**45:**717–719.
26. Wang J, Cai Y, Ren C, Ittmann M. Expression of variant TMPRSS2/ERG fusion messenger RNAs is associated with aggressive prostate cancer. *Cancer Res* 2006;**66:**8347–8351.
27. Yoshimoto M, Joshua AM, Chilton-Macneill S, Bayani J, Selvarajah S, Evans AJ, *et al*. Three-color FISH analysis of TMPRSS2/ERG fusions in prostate cancer indicates that genomic microdeletion of chromosome 21 is associated with rearrangement. *Neoplasia* 2006;**8:**465–469.
28. Demichelis F, Fall K, Perner S, Andren O, Schmidt F, Setlur SR, *et al*. TMPRSS2:ERG gene fusion associated with lethal prostate cancer in a watchful waiting cohort. *Oncogene* 2007;Jan 22 [Epub ahead of print].
29. Bova GS, Parmigiani G, Epstein JI, Wheeler T, Mucci NR, Rubin MA. Web-based tissue microarray image data analysis: initial validation testing through prostate cancer Gleason grading. *Hum Pathol* 2001;**32:**417–427.
30. Rubin MA, de La Taille A, Bagiella E, Olsson CA, O'Toole KM. Cribriform carcinoma of the prostate and cribriform prostatic intraepithelial neoplasia: incidence and clinical implications. *Am J Surg Pathol* 1998;**22:**840–848.
31. Zhou M, Shah R, Shen R, Rubin MA. Basal cell cocktail (34betaE12 + p63) improves the detection of prostate basal cells. *Am J Surg Pathol* 2003;**27:**365–371.
32. Rubin MA, Bismar TA, Andren O, Mucci L, Kim R, Shen R, *et al*. Decreased {alpha-methylacyl CoA racemase expression in localized prostate cancer is associated with an increased rate of biochemical recurrence and cancer-specific death. *Cancer Epidemiol Biomarkers Prev* 2005;**14:**1424–1432.
33. Perou CM, Sorlie T, Eisen MB, van de Rijn M, Jeffrey SS, Rees CA, *et al*. Molecular portraits of human breast tumours. *Nature* 2000;**406:**747–752.
34. Sorlie T, Perou CM, Tibshirani R, Aas T, Geisler S, Johnsen H, *et al*. Gene expression patterns of breast carcinomas distinguish tumor subclasses with clinical implications. *Proc Natl Acad Sci USA* 2001;**98:**10869–10874.
35. Iczkowski KA, Bostwick DG. Criteria for biopsy diagnosis of minimal volume prostatic adenocarcinoma: analytic comparison with nondiagnostic but suspicious atypical small acinar proliferation. *Arch Pathol Lab Med* 2000;**124:**98–107.
36. Arai T, Fujita K, Fujime M, Irimura T. Expression of sialylated MUC1 in prostate cancer: relationship to clinical stage and prognosis. *Int J Urol* 2005;**12:**654–661.
37. Bismar TA, Demichelis F, Riva A, Kim R, Varambally S, He L, *et al*. Defining aggressive prostate cancer using a 12-gene model. *Neoplasia* 2006;**8:**59–68.
38. Saez C, Japon MA, Conde AF, Poveda MA, Luna-More S, Segura DI. Sialomucins are characteristically O-acylated in poorly differentiated and colloid prostatic adenocarcinomas. *Mod Pathol* 1998;**11:**1193–1197.
39. Torbenson M, Dhir R, Nangia A, Becich MJ, Kapadia SB. Prostatic carcinoma with signet ring cells: a clinicopathologic and immunohistochemical analysis of 12 cases, with review of the literature. *Mod Pathol* 1998;**11:**552–559.
40. McNeal JE, Reese JH, Redwine EA, Freiha FS, Stamey TA. Cribriform adenocarcinoma of the prostate. *Cancer* 1986;**58:**1714–1719.
41. McNeal JE, Yemoto CE. Spread of adenocarcinoma within prostatic ducts and acini. Morphologic and clinical correlations. *Am J Surg Pathol* 1996;**20:**802–814.
42. Cohen RJ, McNeal JE, Baillie T. Patterns of differentiation and proliferation in intraductal carcinoma of the prostate: significance for cancer progression. *Prostate* 2000;**43:**11–19.
43. Guo CC, Epstein JI. Intraductal carcinoma of the prostate on needle biopsy: histologic features and clinical significance. *Mod Pathol* 2006;**19:**1528–1535.
44. Bostwick DG, Wollan P, Adlakha K. Collagenous micronodules in prostate cancer. A specific but infrequent diagnostic finding. *Arch Pathol Lab Med* 1995;**119:**444–447.
45. Cerveira N, Ribeiro FR, Peixoto A, Costa V, Henrique R, Jeronimo C, *et al*. TMPRSS2-ERG gene fusion causing ERG overexpression precedes chromosome copy number changes in

prostate carcinomas and paired HGPIN lesions. *Neoplasia* 2006;**8:**826–832.
46. Epstein JI, Fynheer J. Acidic mucin in the prostate: can it differentiate adenosis from adenocarcinoma? *Hum Pathol* 1992;**23:**1321–1325.
47. Goldstein NS, Qian J, Bostwick DG. Mucin expression in atypical adenomatous hyperplasia of the prostate. *Hum Pathol* 1995;**26:**887–891.
48. Ro JY, Grignon DJ, Troncoso P, Ayala AG. Mucin in prostatic adenocarcinoma. *Semin Diagn Pathol* 1988;**5:**273–283.
49. Helpap B. Differential diagnosis of glandular proliferations in the prostate. A conventional and immunohistochemical approach. *Virchows Arch* 1998;**433:**397–405.
50. Amin MB, Schultz DS, Zarbo RJ. Analysis of cribriform morphology in prostatic neoplasia using antibody to high-molecular-weight cytokeratins. *Arch Pathol Lab Med* 1994;**118:**260–264.
51. Epstein JI, Allsbrook WC Jr, Amin MB, Egevad LL. The 2005 International Society of Urological Pathology (ISUP) Consensus Conference on Gleason Grading of Prostatic Carcinoma. *Am J Surg Pathol* 2005;**29:**1228–1242.
52. Wheeler TM, Dillioglugil O, Kattan MW, Arakawa A, Soh S, Suyama K, *et al*. Clinical and pathological significance of the level and extent of capsular invasion in clinical stage T1–2 prostate cancer. *Hum Pathol* 1998;**29:**856–862.
53. Epstein JI, Pizov G, Walsh PC. Correlation of pathologic findings with progression after radical retropubic prostatectomy. *Cancer* 1993;**71:**3582–3593.
54. Bastacky SI, Walsh PC, Epstein JI. Relationship between perineural tumor invasion on needle biopsy and radical prostatectomy capsular penetration in clinical stage B adenocarcinoma of the prostate. *Am J Surg Pathol* 1993;**17:**336–341.
55. Ali TZ, Epstein JI. Perineural involvement by benign prostatic glands on needle biopsy. *Am J Surg Pathol* 2005;**29:**1159–1163.
56. Guerin D, Hasan N, Keen CE. Signet ring cell differentiation in adenocarcinoma of the prostate: a study of five cases. *Histopathology* 1993;**22:**367–371.
57. Bostwick DG, Eble JN. *Urologic Surgical Pathology*. Mosby: St Louis, MO, 1997.
58. Nelson RS, Epstein JI. Prostatic carcinoma with abundant xanthomatous cytoplasm. Foamy gland carcinoma. *Am J Surg Pathol* 1996;**20:**419–426.
59. Tran TT, Sengupta E, Yang XJ. Prostatic foamy gland carcinoma with aggressive behavior: clinicopathologic, immunohistochemical, and ultrastructural analysis. *Am J Surg Pathol* 2001;**25:**618–623.
60. Bostwick DG, Kindrachuk RW, Rouse RV. Prostatic adenocarcinoma with endometrioid features. Clinical, pathologic, and ultrastructural findings. *Am J Surg Pathol* 1985;**9:**595–609.
61. Epstein JI, Woodruff JM. Adenocarcinoma of the prostate with endometrioid features. A light microscopic and immunohistochemical study of ten cases. *Cancer* 1986;**57:**111–119.
62. Ro JY, Tetu B, Ayala AG, Ordonez NG. Small cell carcinoma of the prostate. II. Immunohistochemical and electron microscopic studies of 18 cases. *Cancer* 1987;**59:**977–982.
63. Tetu B, Ro JY, Ayala AG, Johnson DE, Logothetis CJ, Ordonez NG. Small cell carcinoma of the prostate. Part I. A clinicopathologic study of 20 cases. *Cancer* 1987;**59:**1803–1809.